

*Supplementary Information:*

## **Ultrasensitive and Robust Organic Gas Sensors through Dual Hydrogen Bonding**

Jin Zhou<sup>a</sup>, Hongzhen Lin<sup>b</sup>, Xue-Feng Cheng<sup>a</sup>, Jie Shu<sup>c</sup>, Jing-Hui He<sup>a,\*</sup>, Hua Li<sup>a</sup>, Qing-Feng Xu<sup>a</sup>, Na-Jun Li<sup>a</sup>, Dong-Yun Chen<sup>a</sup> and Jian-Mei Lu<sup>a\*</sup>

a. College of Chemistry, Chemical Engineering and Materials Science, Collaborative Innovation Center of Suzhou Nano Science and Technology, National United Engineering Laboratory of Functionalized Environmental Adsorption Materials, Soochow University, Suzhou 215123, P. R. China.

b. *i-LAB, Suzhou Institute of Nano-Tech and Nano-Bionics (SINANO), Chinese Academy of Sciences, Suzhou 215123, P. R. China*

c. *Analysis and Testing Center, Soochow University, Renai Road 199, Suzhou 215123, P. R. China*

Fax: +86 512 65880367; Tel: +86 512 65880368;

E-mail: [jinghhe@suda.edu.cn](mailto:jinghhe@suda.edu.cn); [lujm@suda.edu.cn](mailto:lujm@suda.edu.cn)

### **Experimental Procedures**

*Materials and Device Measurements:* 4, 4'-azodoaniline and Squaric acid were obtained from Alfa Aesar (China) Chemicals Co., Ltd (Shanghai, China) and Shanghai Macklin Biochemical Co. Ltd, respectively. UV-vis absorption spectra were measured at room temperature using a Shimadzu UV-3600 spectrophotometer. XRD measurements were carried out using a Multiple Crystals X-ray Diffractometer (X'Pert PRO, PANalytical). The different gas flow rate was controlled by a PERMEATER (PD-1B-2). Electric gas sensing data were recorded using a semiconductor characterization system (Keithley 4200-SCS) under a fixed total flow (300 sccm) of different concentrations of target gas. Solid-state NMR (SSNMR) experiments were performed on a Bruker Advance III HD 400 spectrometer. 1D

$^{13}\text{C}\{^1\text{H}\}$  cross-polarization (CP)/MAS spectra were recorded using a CP contact time of 1.5 ms, a recycle delay of 5 s and 1024 scans with a SPINAL-64 high power  $^1\text{H}$  decoupling sequence during acquisition. 2D  $^{13}\text{C}$ - $^1\text{H}$  frequency-switched Lee-Goldburg heteronuclear correlation (FSLG-HETCOR) experiments were conducted using a CP contact time of 1.5 ms, a recycle delay of 3 s with 128 scans for a total of 86 t1 increments. The sum frequency generation (SFG) spectrometer laser system was set up by EKSPLA. The incident angle of the visible beam is  $60^\circ$ , and the incident angle of the infrared beam is  $55^\circ$ . The IR pulses around  $2750\text{-}3000\text{ cm}^{-1}$  and the visible signal at 532 nm are about 25 ps at 50 Hz. The energy of the visible and IR beams is generally less than 20 mJ, the photo-damage of studied sample can be ignored during examination process.

*Synthesis of Poly(4,4'-azodianiline-squaraine)*: 4, 4'-azodianiline 500 mg (2.36 mmol) and squaric acid 300 mg (2.63 mmol) were dissolved in 35 mL n-butanol or other mixed solvents in a three-neck flask. The mixture was then refluxed and stirred at  $130^\circ\text{C}$  for 2-18 h. After being cooled to room temperature, the mixture was filtered and washed using tetrahydrofuran 10 times. The obtained PADS was dried in a vacuum oven at  $70^\circ\text{C}$  for 12 h, as shown in **Fig. 1**. The product was obtained as a kermesinus powder.

*Sensor Preparation*: The process for fabricating sensors is as follows: 50 mg of PADS was mixed with 1 mL of absolute ethanol to form a paste, which was then brush-coated onto an  $\text{Al}_2\text{O}_3$  substrate printed with five pairs of Ag-Pd interdigitated electrodes (IDES, electrode distance and width were both  $200\ \mu\text{m}$ ) ( $14\ \text{mm}\times 7\ \text{mm}$ ,  $0.64\ \text{mm}$  in thickness) to form a sensitive film ( $\sim 200\ \mu\text{m}$  in thickness) before being air dried at  $70^\circ\text{C}$  for 2 h. The appearance of the sensor device is shown in **Fig. S3**, and the elements mapping image of sensor device based on PADS is shown in **Fig. S4**.

*Sensing Measurements:* The performance of the sensor based on PADS was characterized by measuring the current caused by different gas concentrations. The changes in the current were monitored through DC current–voltage (I–V) measurements using a Keithley 4200, specifically, placing the sensor in a sealed 1200 mL chamber with an electric feed-through a gas inlet and a gas outlet, respectively. A schematic diagram of the sensing system is shown in **Fig. S7** and **S8**. For the purposes of ensuring accurate experimental data and that target gas was completely in the chamber, the time gap of every single I–V characteristics was four minutes. Before the target gas was put into chamber, the chamber was purged with pure nitrogen to ensure the current of on the sensor remained stable. To reduce the impact of the rate of airflow, the rate of the airflow was controlled at a rate of 300 mL/min. Nitrogen gas was used as a carrier to dilute the NH<sub>3</sub> and NO to the desired concentrations and the operating temperature was maintained at room temperature (25 °C). Most organic chemiresistors require more than half an hour to response and recover, in order to carry out measurements and compare the response in a more convenient way, the exposure time was chosen as 4 min, the purging time was fixed at 10 min per pulse.<sup>[1]</sup>

*Theoretic calculation:* All density functional theory calculations (DFT) were performed based on a level of GGA- UBLYP/DNP implemented in DMol<sup>3</sup> code<sup>[2]</sup>. Hydrogen bonding and van der Waals (vdW) interactions were semi-empirically corrected by Tkatchenko-Scheffler (TS) scheme.<sup>[3]</sup> Several initial adsorption models were estimated considering NH<sub>3</sub> and NO adsorbed to all possible sites of the N atom in the PADS. These models were optimized until converging within a criteria of  $1 \times 10^{-5}$  eV in energy and 0.02 eV/Å in residue force. Charge populations were analyzed using a Hirshfeld partitioned scheme.



**Fig. S1** Image of the PADS powder.

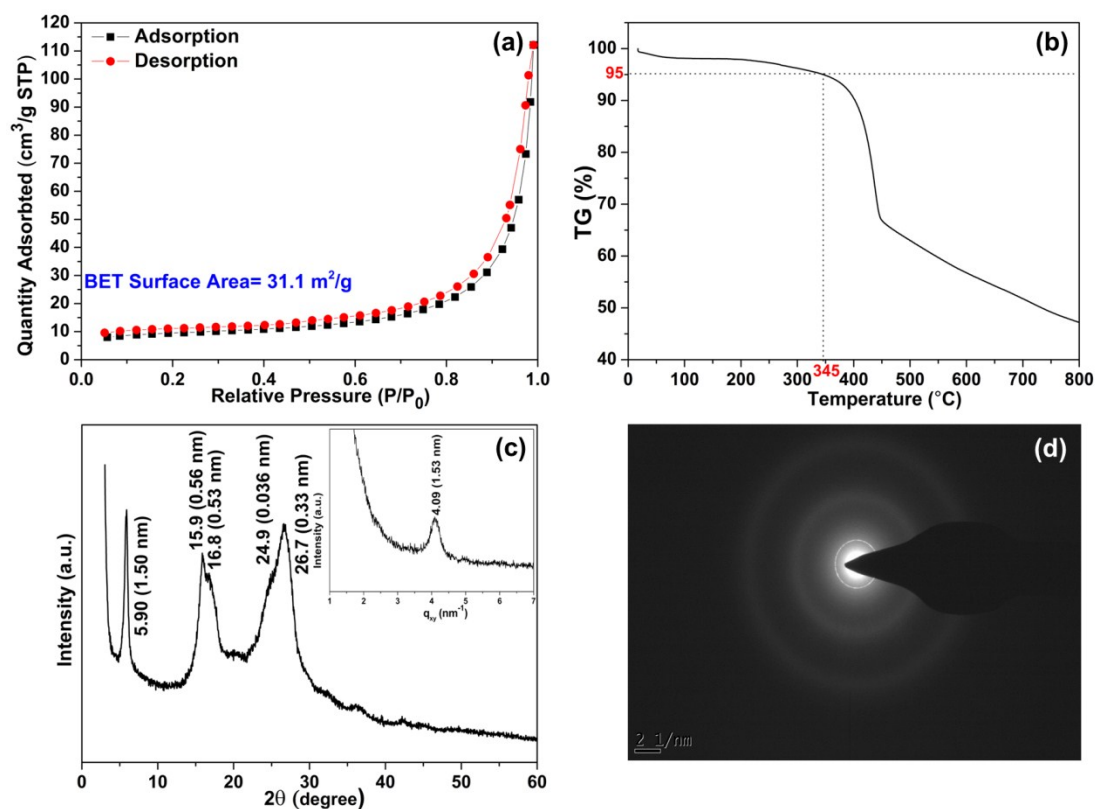


**Fig. S2** (a) Nitrogen adsorption–desorption isotherms of PADS. (b) Thermogravimetric analysis curve of PADS. (c) XRD patterns of PADS and the spectra of SAXS of PADS. (d) Selected area electron diffraction (SEAD) image of PADS.

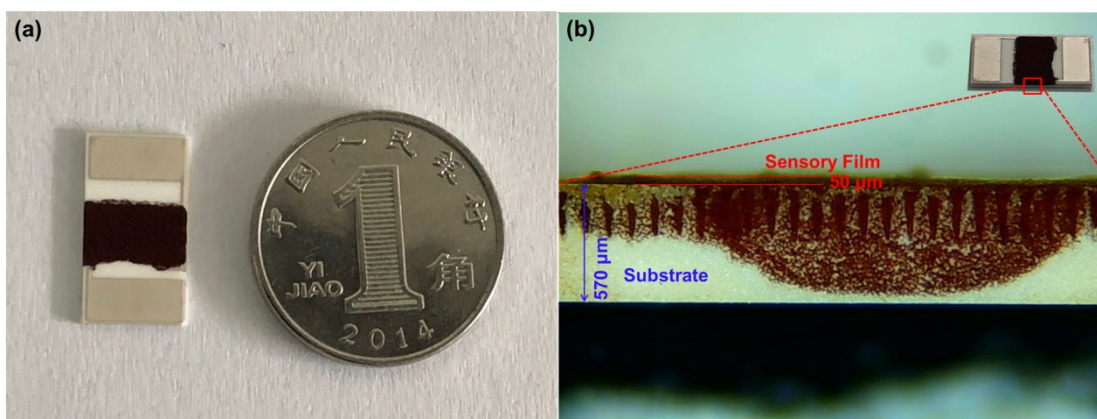


**Fig. S3** (a) Appearance of sensor based on PADS. (b) The thickness of the sensory film.

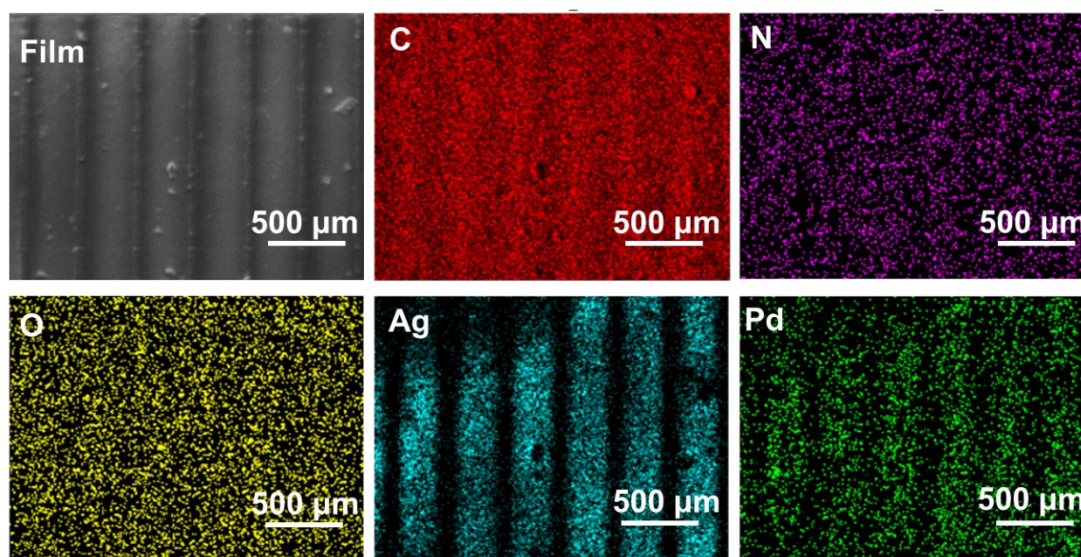


**Fig. S4** Elements mapping image of sensor device based on PADS.

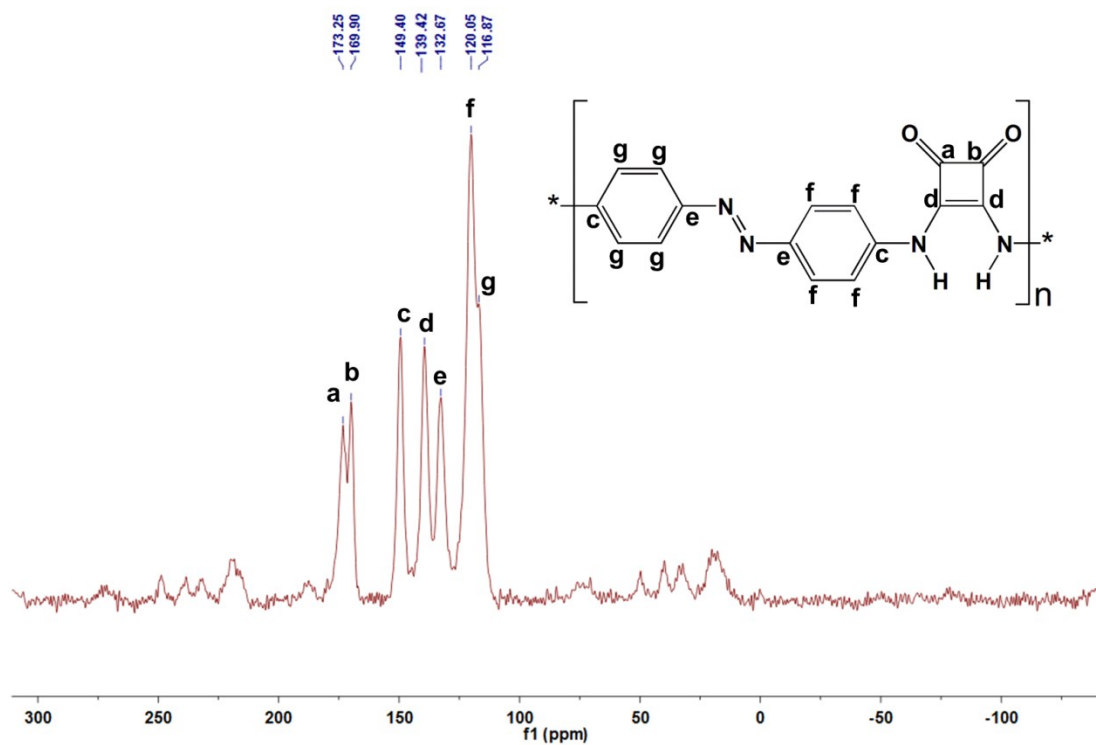


**Fig. S5** Solid-state NMR  $^{13}\text{C}$  cross polarization spectrum of PADS. Peaks are assigned using the alphabet labels with respect to the structural scheme.

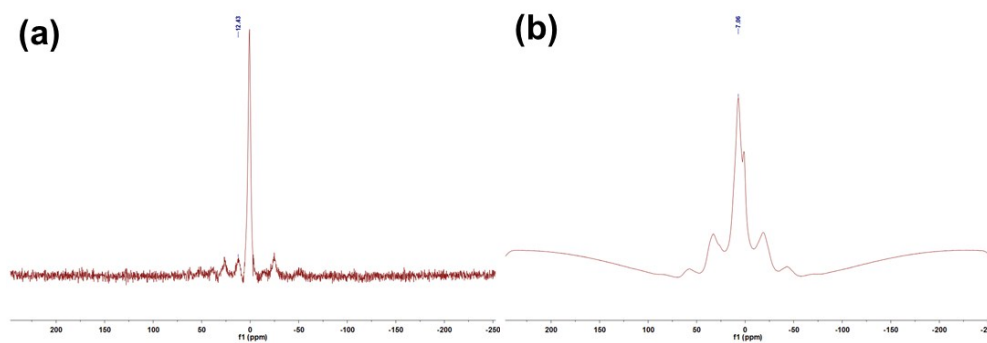


**Fig. S6** Solid-state NMR 1D  $^1\text{H}$  spectra of PADS. (a) Double quantum filtered  $^1\text{H}$  spectrum. (b) One pulse excited  $^1\text{H}$  spectrum.

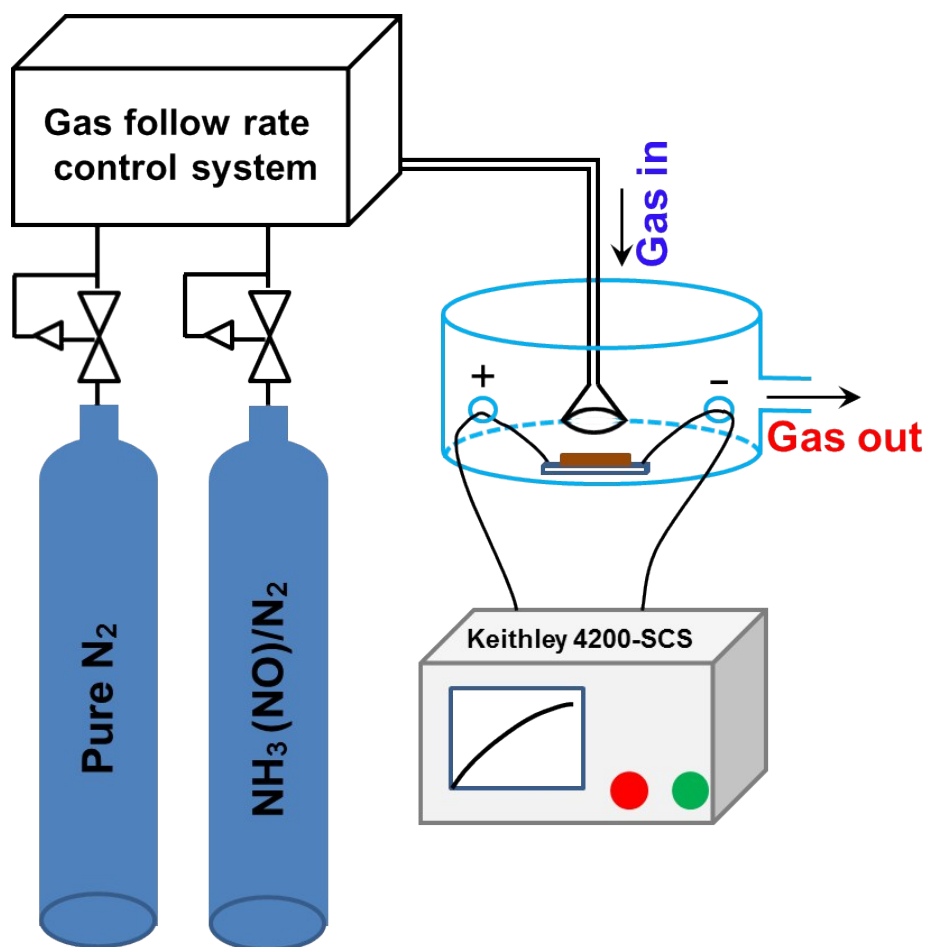


**Fig. S7** Schematic of gas chamber for gas sensing measurements.

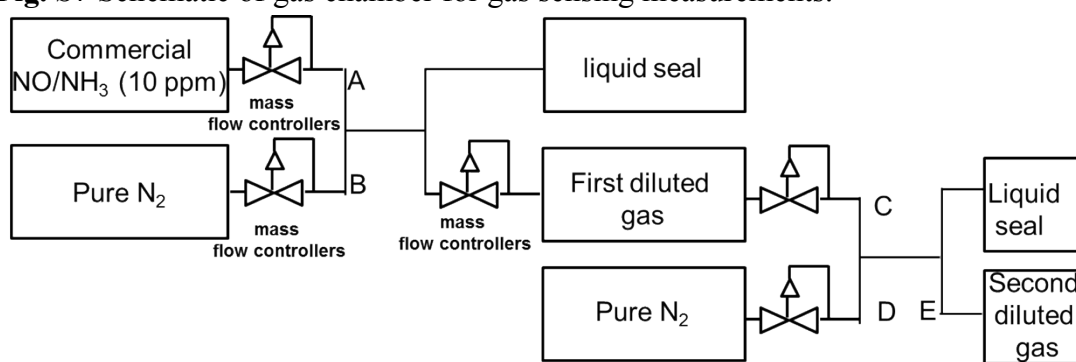


**Fig. S8** The schematic diagram of the gaseous diluting method.

**Table S1.** The rate of gas flow corresponding to Fig. S8 which used to dilute to different gas concentration.

A	B	C	D	E
9.999 SLM/min	1 SCCM/min	10 SCCM/min	0.99 SLM/min	10 ppt
9.999 SLM/min	1 SCCM/min	/	0	1 ppb
9 SLM/min	1 SLM/min	/	0	1 ppm

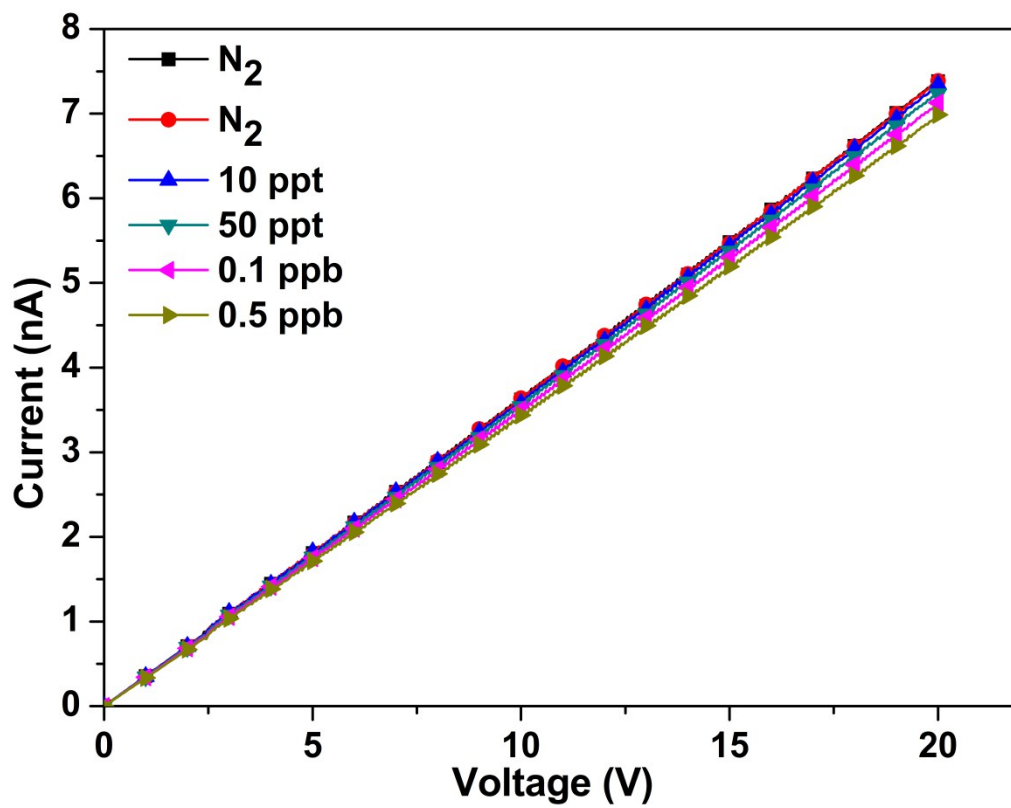


**Fig. S9** The I–V characteristics of the sensor based on PADS exposure to ultra-low concentration of  $\text{NH}_3$ .

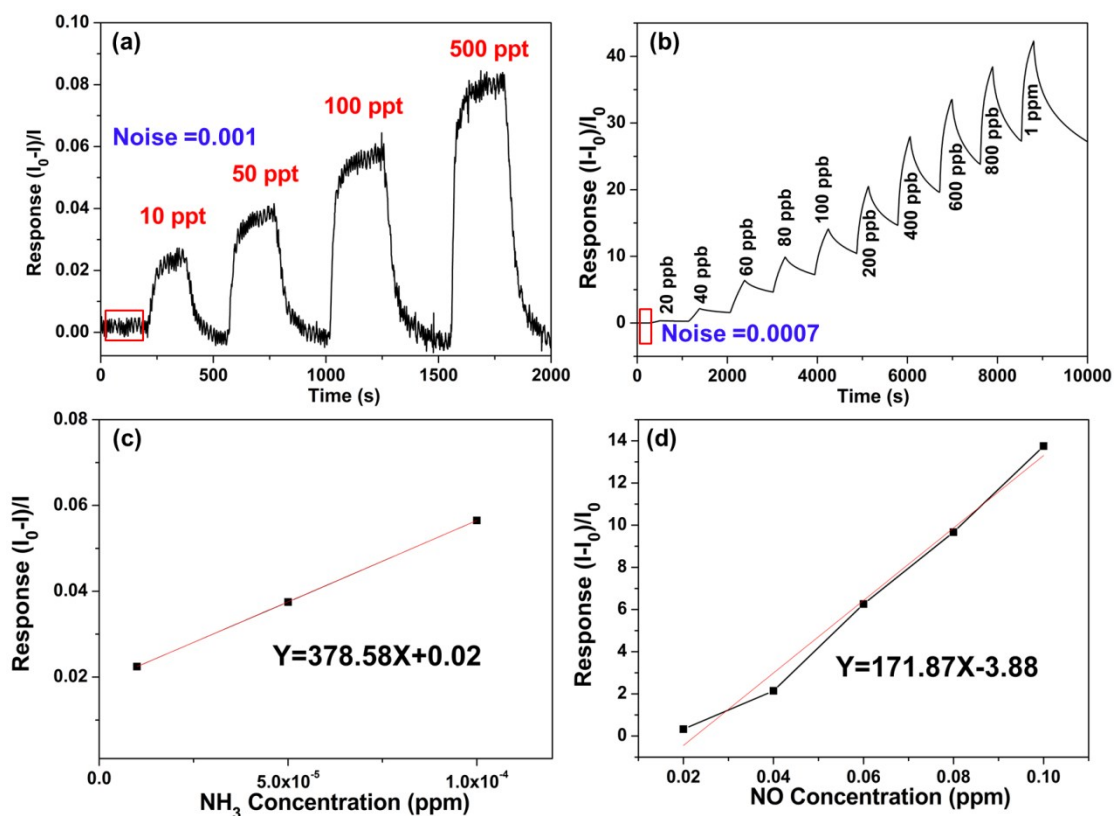


**Fig. S10** (a) Noise during detection of  $\text{NH}_3$  and (b) NO. (c) The linear fitting of sensor response towards  $\text{NH}_3$  and (b) NO. The noises of 0.001 and 0.0007 were extracted from baseline before  $\text{NH}_3$  and NO exposure, respectively. Hence, the  $\text{LOD}=3 \text{ SD}/m=3*0.001/378.58= 8 \text{ ppt}$  in detect ammonia was calculated. Similarly, a LOD of 12 ppt was calculated in detect nitric oxide.

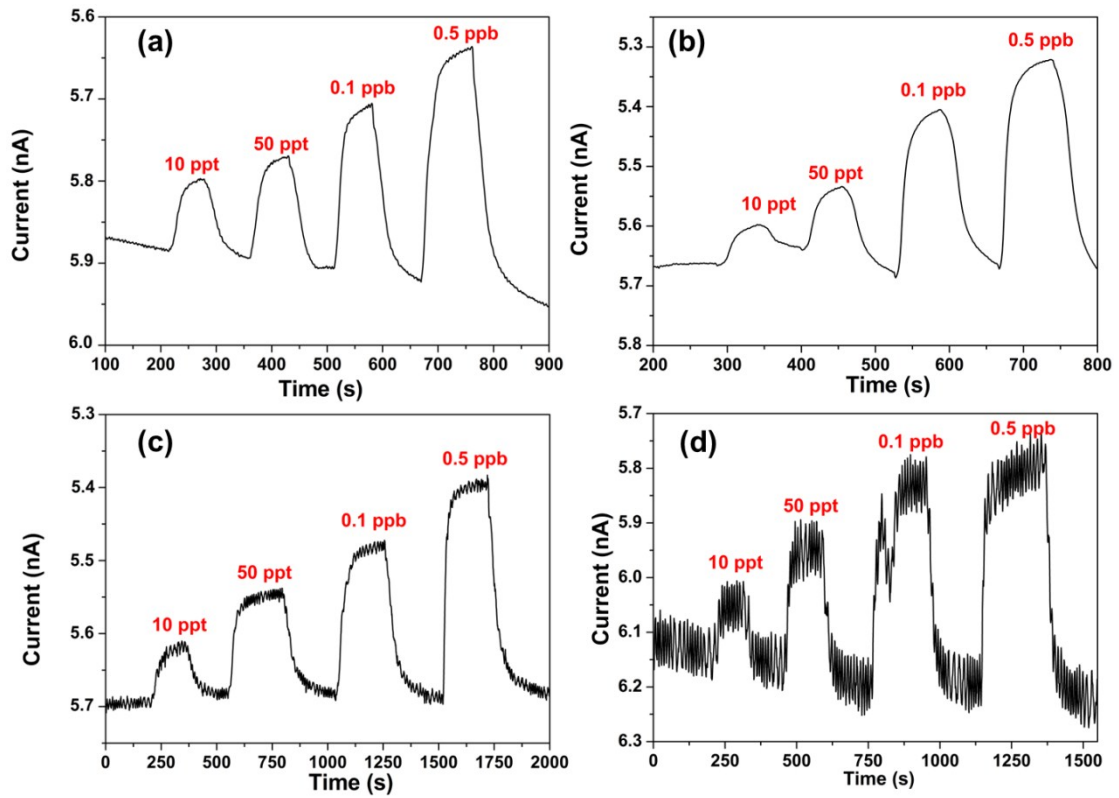


**Fig. S11.** Temporal response of the sensor 2, sensor 3, sensor 4 and sensor 5 based on PADS exposure to ultra-low concentration of  $\text{NH}_3$ .

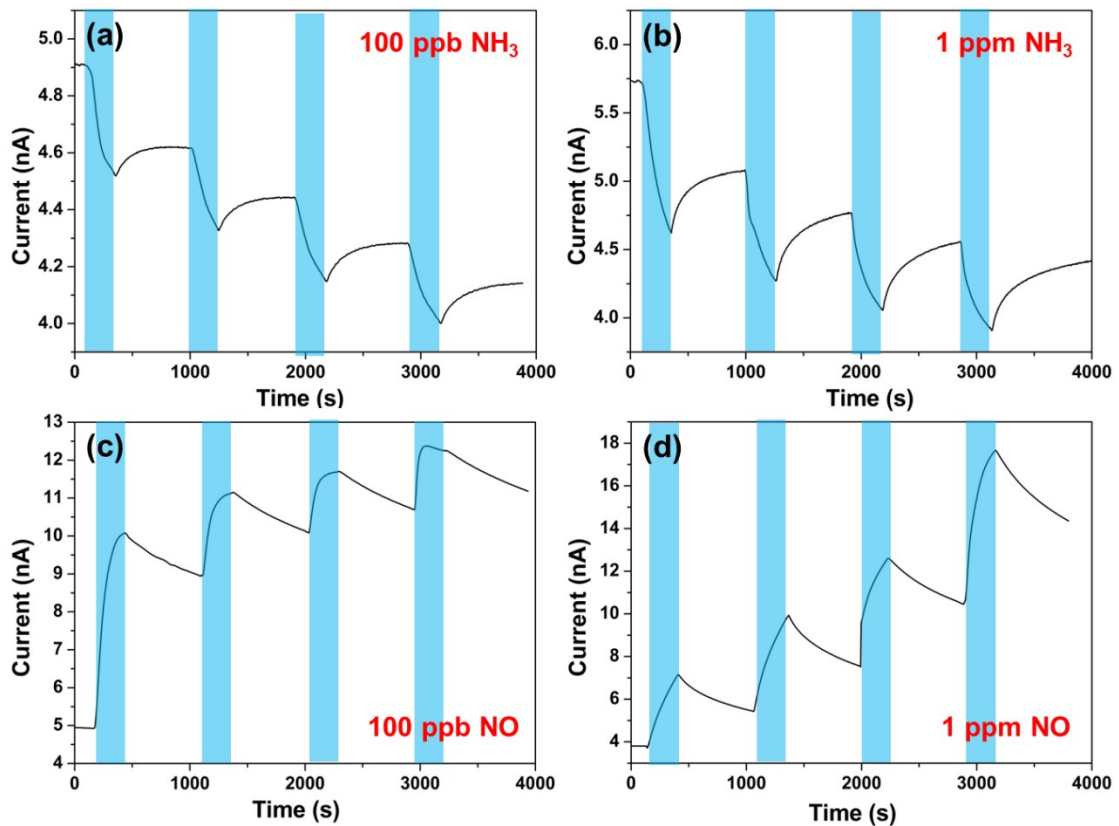


**Fig. 12** The repeatability of the sensor at 100 ppb/1 ppm  $\text{NH}_3$  and NO.

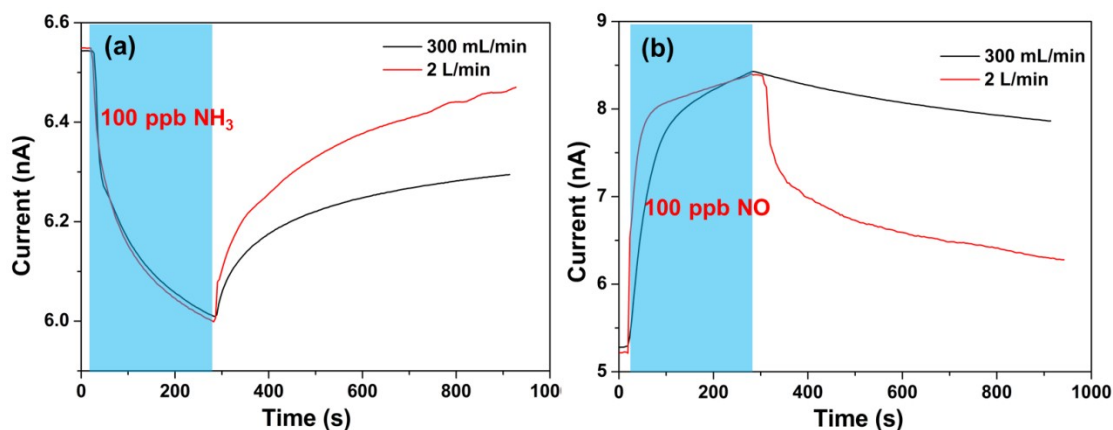


**Fig. S13** Effects of different flow drying air flow on the recoverability of the sensor.

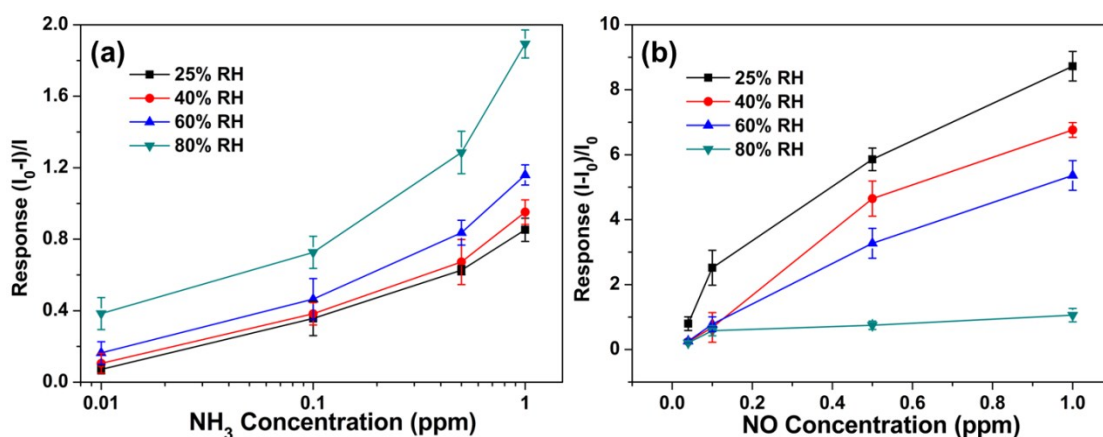


**Fig. S14** Effect of environmental humidity to sensor based on PDBS. (a) Response of sensor based on PDBS at different NH<sub>3</sub> concentration at different humidity. (b) Response of sensor based on PDBS at different NO concentration at different humidity. The error bars refer to the standard error of three successive tests at same relative humidity or gas concentration.

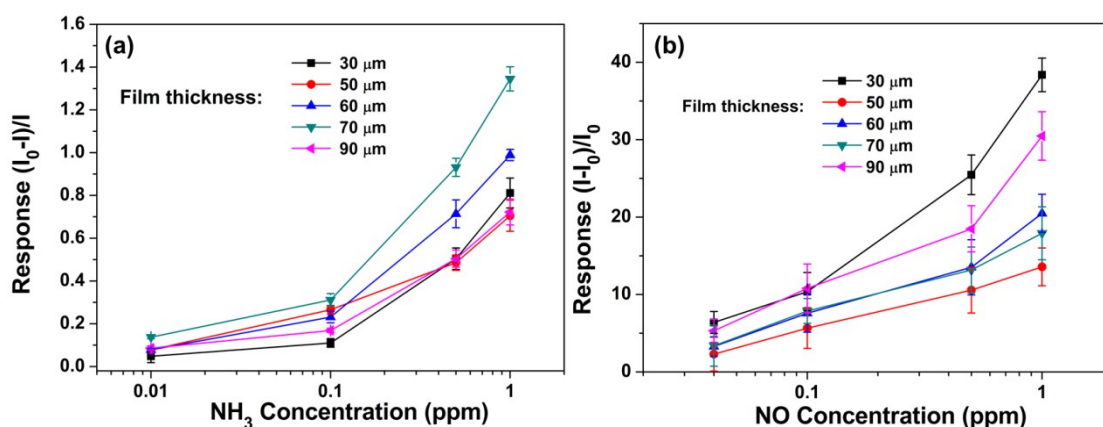


**Fig. S15** Response of a series of films with different sensing film thicknesses towards (a) NH<sub>3</sub> and (b) NO.

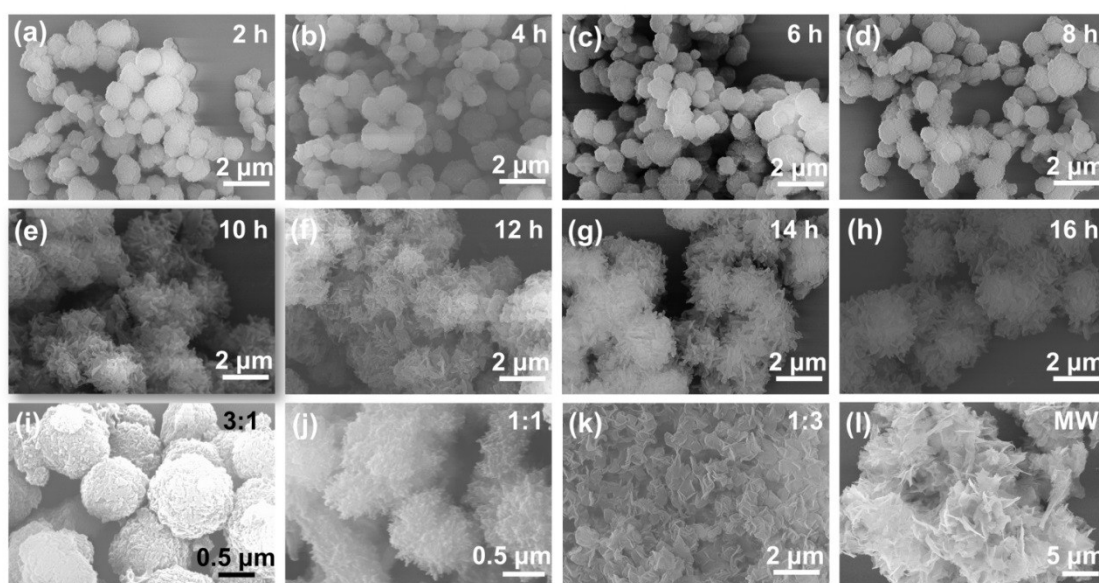


**Fig. S16** SEM images of PADS at different reaction times of 2 h (a), 4 h (b), 6 h (c), 8 h (d), 10 h (e), 12 h (f), 14 h (g) and 16 h (h), respectively. SEM images of PADS obtained from different solvents: o-dichlorobenzene and n-butanol with the volume ratio of 3:1 (i), 1:1 (j), 1:3 (k). And SEM image of PADS synthesized by microwave method (l).

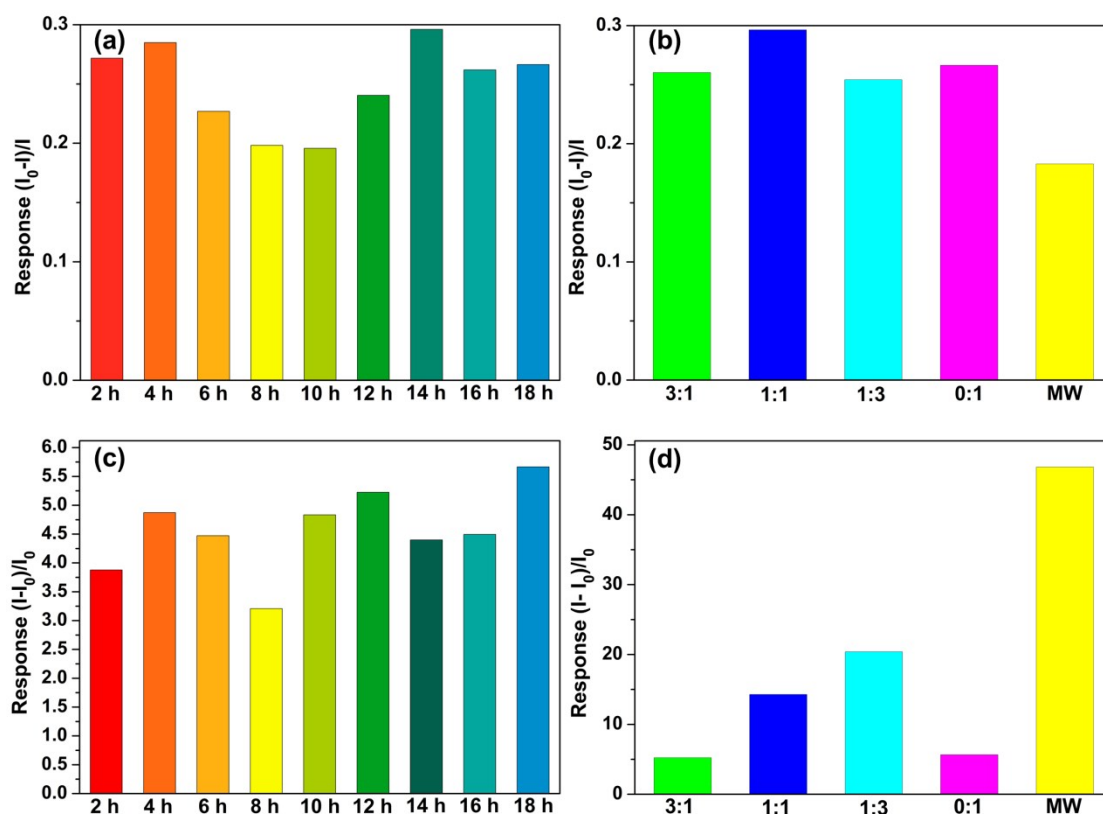


**Fig. S17** Performance of the sensors prepared using different PADS samples (a) Response to 100 ppb of ammonia for PADS with different reaction periods and (b) different solvents and methods. (c) Response to 100 ppb of NO for PADS with different reaction periods and (d) different solvents and methods. The ratios of 3:1,

1:1, 1:3 and 0:1 refer to Vo-dichlorobenzene:Vn-butanol. MW is referred to the microwave method.

**Table S2.** Binding Energies of NH<sub>3</sub> adsorbed on PADS oligomer in different models. The details geometries of these models are illustrated in **FigureS18**.

Model name	Binding energy (eV)	Binding-configuration
0	0.00	None-Interaction for BSSE correction
A	0.17	No substantial bonding
B	0.20	No substantial bonding
C	0.11	No substantial bonding
D	0.20	No substantial bonding
E	<b>0.71</b>	<b>Dual hydrogen bonding</b>
F	0.22	N=N...H-NH <sub>2</sub> Hydrogen bonding
G	<b>0.73</b>	<b>Dual hydrogen bonding</b>

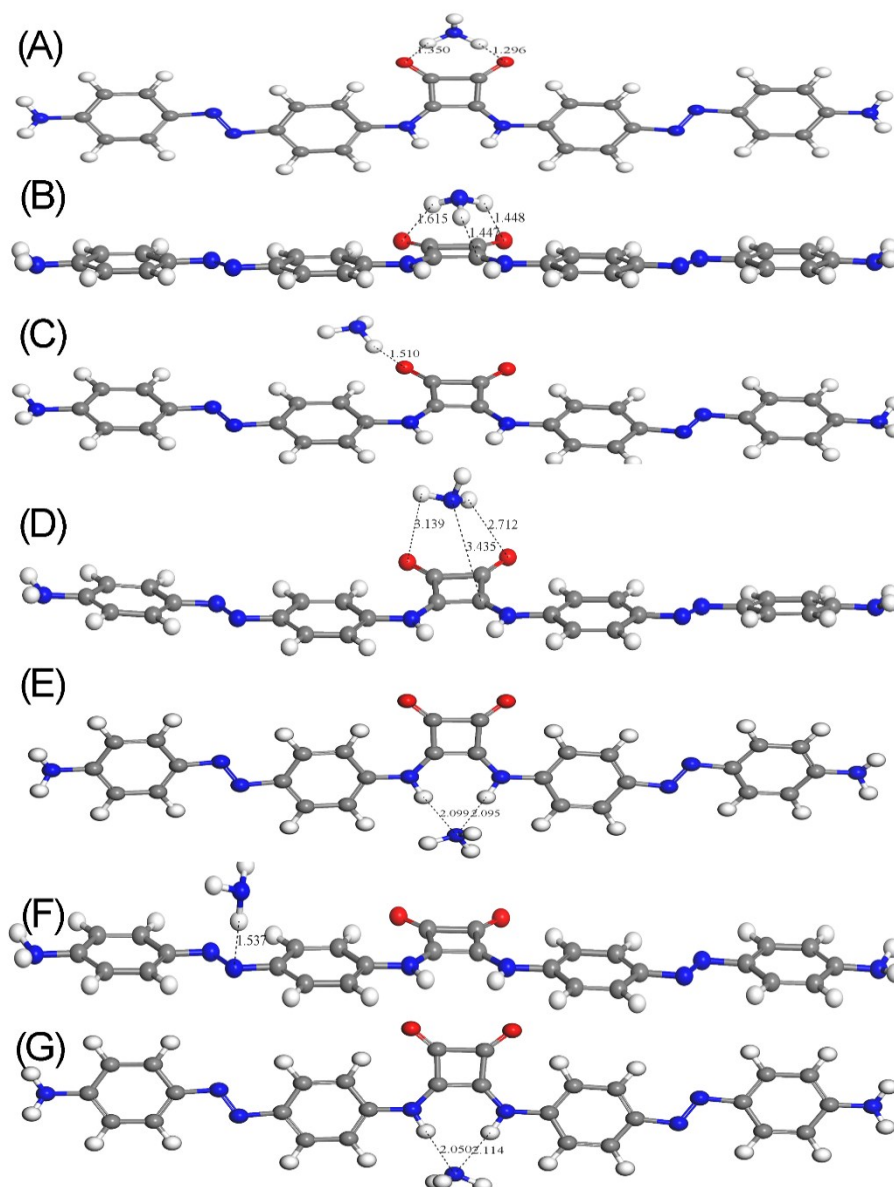


**Figure S18.** Proposed binding models of ammonia on a PADS chain. These models correspond to the entries from A to G in **Table S2**.

**Table S3.** Binding Energies of NO adsorbed on PADS chain in different models. The details geometries of these models are illustrated in **FigureS19**

Model name	Binding energy (eV)	Binding-configuration
0	0.00	None-Interaction for BSSE correction
A	0.17	No substantial bonding
B	0.05	No substantial bonding
C	<b>0.41</b>	<b>Dual hydrogen bonding</b>
D	0.24	Azo $N\cdots N-O$ weak interaction
E	0.08	No substantial bonding
F	0.13	No substantial bonding

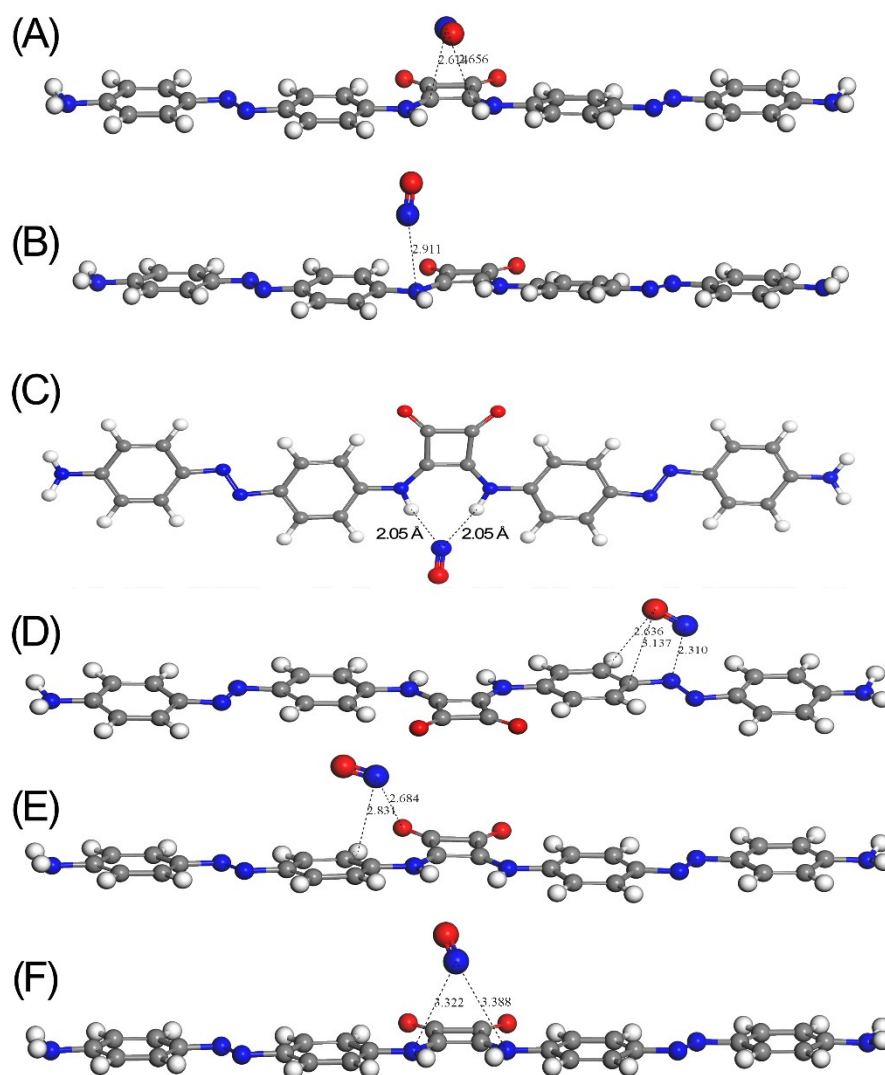


**Figure S19.** Proposed binding models of nitric oxide on a PADS chain. These models correspond to the entries from A to F in **Table S3**.

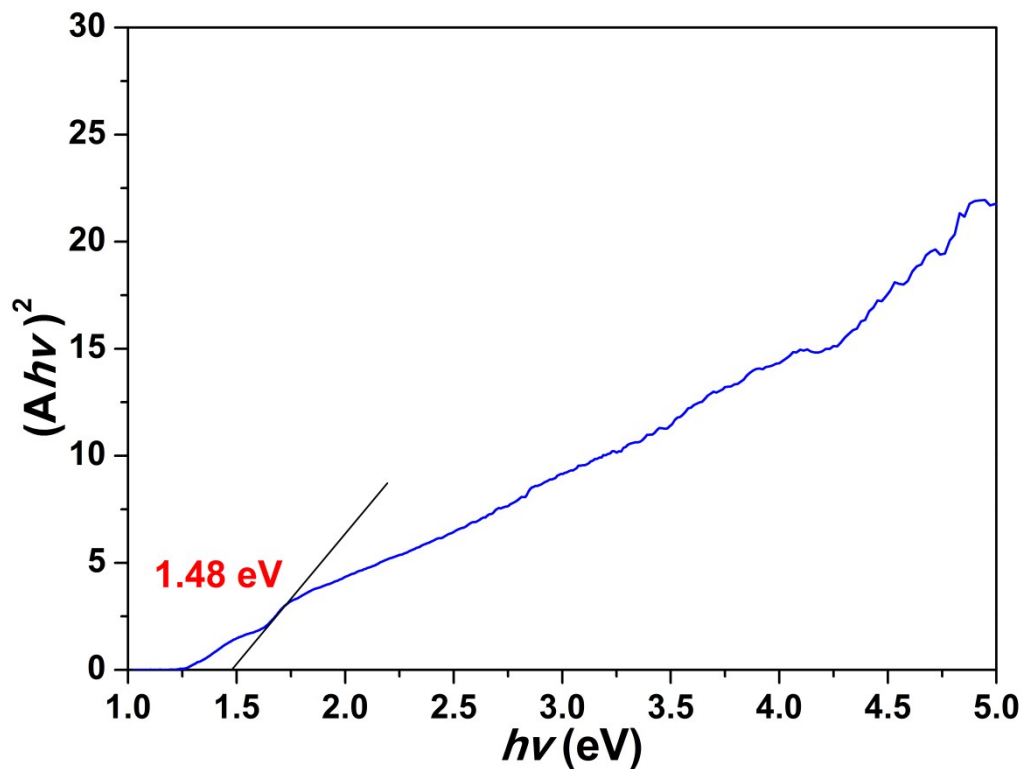


Fig. S20. The Tauc plot of PADS from solid UV-vis spectra.

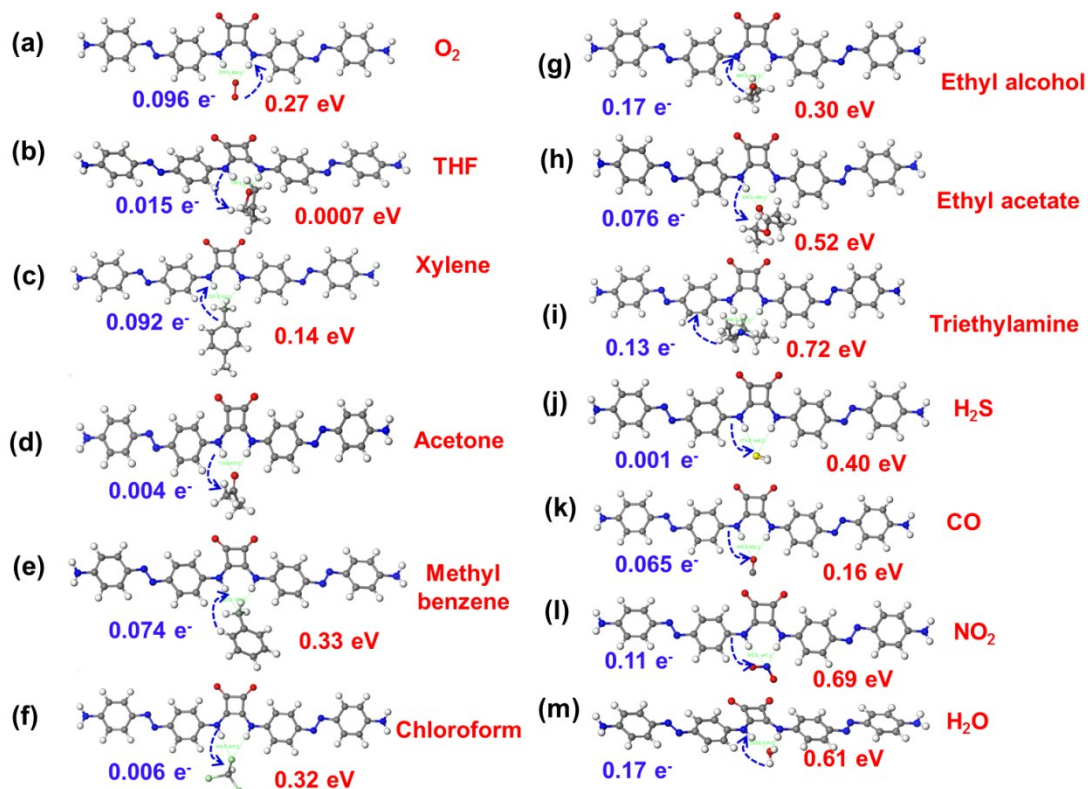
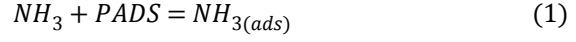


Fig. S21 Binding Energies and charge transfer of different analytes adsorbed on PADS.

## Appendix: Detailed deduction of sensitivity enhancement from DHB

Under the dynamic equilibrium between the PADS surface the gas flow with a certain ammonia concentration  $[NH_3]$ , the chemically adsorbed ammonia is proportional to  $[NH_3]$  and its affinity  $k$  that depends on the reaction free energy change:



$$k = \frac{\theta_{NH_{3(ads)}}}{[NH_3]} \quad (2)$$

$$\ln k = -\frac{\Delta G}{RT} \cong -\frac{\Delta H + \Delta nRT}{RT} \quad (3)$$

Where  $\theta_{NH_{3(ads)}}$  is the coverage of chemically adsorbed ammonia on PADS surface,  $k$  is the equilibrium constant to represent surface affinity,  $\Delta G, \Delta H, R, T$ , are free energy change, enthalpy change, gas constant and temperature, respectively.

In the double Schottky mode, the gas affinity enter into the power law of response:

$$S = \frac{I_0}{I} = \frac{R}{R_0} = \frac{[k[NH_3]]^n}{\omega} \quad (4)$$

where  $\omega$  is the depletion layer depth and  $n$  is the power factor. Under an simple assumption that both SHB and DHB models has same charge transfer effect from ammonia to PADS and using other typical parameters, a discrepancy in the binding energies will bring huge discrimination in affinity by a factor of :

$$\frac{k_{DHB}}{k_{SHB}} = \exp\left(-\frac{\Delta G_{DHB} - \Delta G_{SHB}}{RT}\right) = \exp\left(-\frac{\Delta H_{DHB} - \Delta H_{SHB}}{RT}\right) = 440000 \quad (5)$$

This improved affinity will finally bring a dramatic enhancement of response in our PADS gas sensor.

$$\frac{S_{DHB}}{S_{SHB}} = \left(\frac{k_{DHB}}{k_{SHB}}\right)^n = 440000^{0.43} = 267 \quad (6)$$

## References

- [1] aF. Zhang, G. Qu, E. Mohammadi, J. Mei, Y. Diao, *Advanced Functional Materials* **2017**, 27; bZ. Wang, L. Huang, X. Zhu, X. Zhou, L. Chi, *Advanced materials* **2017**, 29.
- [2] B. Delley, *The Journal of Chemical Physics* **2000**, 113, 7756-7764.
- [3] A. Tkatchenko, M. Scheffler, *Physical Review Letters* **2009**, 102, 073005.